Synthesis of the $Bi_2Sr_2CaCu_2O_{8+\delta}$ superconductor following a polymer matrix route

A. SOTELO, J. I. PEÑA, L. A. ANGUREL*, C. DIEZ, M. T. RUIZ, G. F. DE LA FUENTE, R. NAVARRO
Instituto de Ciencia de Materiales de Aragón (Consejo Superior de Investigacienes Cientificas–Universidad de Zaragoza) Mª de Luna, 3 E-50015 Zaragoza, Spain

This paper presents a convenient polymer matrix synthesis route based on the use of metal acetates, which yields $Bi_2Sr_2CaCu_2O_{8+\delta}$ (2212 phase) with a T_c higher than 93 K, in air and within a short sintering time (6–12 h) at 855 °C. The phase quality of the intermediate and final products has been analysed by powder X-ray diffraction and scanning electron microscopy with energy-dispersive spectroscopy. Macroscopic superconducting characteristics have been determined by alternating-current magnetic susceptibility and direct-current magnetization. The results obtained on a large number of samples suggest that this preparation route is highly reproducible and leads to black-grained powders with excellent homogeneity within a relatively short processing time. The usefulness of these powders to obtain textured superconducting products has been explored and representative results are presented here.

1. Introduction

Since the discovery of superconductivity in the Bi–Sr–Cu–O system by Michel *et al.* [1] and the subsequent work reported by Maeda *et al.* [2] on superconductivity at attractively high critical temperatures, T_c in the rare-earth-free system Bi–Sr–Ca–Cu–O (BSCCO), much work has been performed searching for nominal stoichiometries that yield a single-phase polycrystalline material with a well-defined T_c. BSCCO compounds were observed to contain three different superconducting phases possessing approximate T_c values of 20 K (the 2201 phase), 90 K (the 2212 phase) and 110 K (the 2223 phase). The 2201 and 2212 phases are relatively easy to synthesize, because they are thermodynamically stable over a wide range of temperature and stoichiometric range within the Bi_2O_3–SrO–CaO–CuO system. In contrast, the 2223 phase is stable only over a narrow temperature range and exhibits phase equilibria with fewer compounds of the BSCCO system [3].

The 2212 superconductor offers several advantages over the 2223 phase. These include a considerably extended single-phase region for $Bi_xSr_{3-y}Ca_yCu_2O_{8+\delta}$ where $x = 2$–2.35 and $y = 0.7$–1 which allows its relatively rapid preparation with higher degrees of phase purity and homogeneity than the 2223 phase, and improved stability to moisture, among other factors [3, 4]. On the other hand, its lower critical temperature poses, in principle, an important disadvantage when considering its potential for devices operating at 77 K. Nevertheless, since short-term applications for these high-T_c materials are being considered at temperatures below 65 K, the study of the 2212 phase superconductor and its preparation using simple and reliable routes are still of significant importance at this time.

While improved solid-state reaction methods have been developed based on the use of intermediate precursors, such as the compound Bi_2CuO_4 [5], as well as on the adequate choice of stoichiometry [6], polycrystalline BSCCO (2212) samples obtained using similar conventional solid-state reaction methods usually exhibit resistive transition temperatures $T_{cR} = T_c(R = 0)$ lower than 85 K [7]. Values of T_{cR} greater than 85 K have been reached [7–9] using wet preparative routes to obtain an intimate mixture for calcination, combined with reducing atmospheres during the subsequent sintering process. The addition of specific amounts of lead also improve T_c by about 5 K. Nevertheless, a lead-free 2212 phase with T_{cR} values up to 93 K has been prepared [10] by controlling the oxygen content and the structural characteristics to maximize T_{cR}. The presence of excess oxygen intercalated in Bi–O redox layers has been found to limit T_{cR} for the 2212 phase. A suitable nitrogenation procedure has made it possible to optimize T_{cR} to 96 K (with a transition width of 3 K) for single-phase BSCCO (2212) [11].

Measurements of alternating-current (a.c.) susceptibility $\chi_{a.c.}(T)$ and direct-current (d.c.) magnetization, $M(T)$, have been widely used in the characterization of high-temperature superconducting powdered

* To whom correspondence may be addressed.

0022–2461

samples, especially to determine T_c, which is defined in the literature using different criteria. The onset temperature, T_{on}, of diamagnetism [12, 13], which depends on the sensitivity of the particular experimental apparatus used and on the superconducting phase content, has been used in some instances to define T_c. In other contributions it has been defined as the temperature, T_{cM}, for which a certain percentage (about 1%) of the measured magnitude is reached [14].

T_{cM} clearly depends on the chemical composition of the 2212 phase, which in turn influences its structure. For example, T_{cM} increases significantly with decreasing Ca and Bi content. Furthermore, samples with Sr-rich compositions ([Sr]/[Ca] = 2.2/0.8) and intermediate Bi contents, sintered in air at 870 °C, exhibit very high T_{cM} values (93 K) [4]. It has also been established that T_{on} and T_{cM} depend strongly on the oxygen content and can reach values as high as 95 K [12–14].

This paper reports results obtained with a simple polymer matrix method [15] that yields homogeneous lead-free superconductor powder (2212 phase) with T_{on} and T_{cM} values as high as 94 K and 91.5 K, respectively, after only a relatively short sintering time in air without any need to control the oxygen partial pressure during thermal processing.

2. Experimental procedure

The polymer matrix procedure followed, described in detail elsewhere [15, 16], has been carried out as previously reported for BSCCO (2223) [17, 18]. $Bi(CH_3COO)_3$ (Alfa; purity, 99.99%), $Sr(CH_3COO)_2 \cdot \frac{1}{2}H_2O$ (Johnson Matthey; purity, 99.99%), $Ca(CH_3COO)_2 \cdot H_2O$ (Aldrich; purity 99%) and $Cu(CH_3COO)_2 \cdot H_2O$ (Aldrich; purity, 98 + %) were dissolved in a mixture of acetic acid and distilled water. To this light-blue solution, another solution of polyethylenimine (Aldrich; 50 wt% in water) in distilled water was added and the former solution turned royal blue immediately. The resulting combined solution was evaporated in the rotary evaporator, heated to decomposition on a hot plate and calcined in a furnace for 12 h at 750 °C. The resultant powder agglomerate was ball milled for 1 h, sintered at 820 °C for 12 h and, after $\frac{1}{2}$ h of remilling, it was pressed and sintered for a second time at 855 °C for 1, 3, 6, 12, 60 and 100 h in air.

The phase composition was determined by powder X-ray diffraction (XRD) using a Rigaku DMAX-B system with rotatory Cu anode, coupled to a goniometer with graphite monochromator for selecting the Cu Kα wavelength. Superconducting and secondary-phase concentrations were estimated from the contribution of the area of the peaks of each phase to the overall diffractogram.

The microstructure of the samples has been studied by means of scanning electron microscopy (SEM) (JEOL microscope model JSM 6400) equipped with a Si(Li) energy–dispersive spectroscopy (EDS) (Link Analytical eXL) system. To perform elemental microanalysis (EDS by SEM), the samples were polished by conventional techniques down to a roughening of 0.3 μm. These microanalyses were performed using 20 keV energy electrons and a beam current of 6×10^{-10} A. In addition, powdered samples were suspended in isopropyl alcohol, deposited over metallic sample holders under an ultrasonic bath, dried and covered with a Au layer. These samples were observed by SEM to determine their characteristic morphology and particle size.

Macroscopic superconducting properties were determined on powdered samples by measuring the in-phase component χ', and out-of-phase components, χ'', of $\chi_{a.c.}(T)$, in a fully automated susceptometer [19] using an a.c. field amplitude of 5.5 Oe and a frequency of 119 Hz. From these data the position of the critical temperature may be deduced as well as the quality and homogeneity of the superconducting phase.

The values of the onset temperatures, T_{on} and T_{cM}, have been determined here using the following criteria. T_{on} has been defined from the extrapolation of the two highest temperatures for which the diamagnetic $\chi'(T)$ signal is clearly above the experimental noise level to the $\chi' = 0$ limit. T_{cM} represents the temperature at which the relationship $\chi'(T_{cM}) = \chi'(4.2\text{ K})/100$ holds. Although the T_{cM} values defined in this manner are a function of h_0 values, for powdered samples and in the range used in the experiment, this dependence is very low; it nevertheless must be taken into account.

In addition, to analyse the differences associated with the intragranular superconducting properties, isothermal measurements of the d.c. magnetization, $M(T, H)$, were performed at low temperatures using a superconducting quantum interference device (SQUID) magnetometer (Quantum Design). All these measurements were performed under zero-field-cooled conditions, without compensation for the background fields.

3. Results and discussion

3.1. Powder X-ray diffraction analysis

The evolution of the XRD patterns after calcination and sintering is presented in Fig. 1 and summarized in Table I for the samples studied (the pattern-matching procedure has been used for peak identification). These data suggest that the polymer matrix preparation route induces, through an effective pyrolysis process, rapid formation of the 2212 phase, since 75% of the product obtained after the first sintering period of 12 h at 820 °C correspond to this phase. Furthermore, after a second sintering period at 855 °C, the amount of 2212 phase in these samples ranges from 86% (1 h) to 93% (100 h). Simultaneously, the amount of accompanying secondary phases decreases accordingly. The main difference between the samples sintered 855 °C for different time lengths is not their phase composition, but rather their relative degree of crystallinity, as deduced from the XRD peak widths. Samples that have been sintered for longer periods of time thus exhibit narrower peaks in their pattern (i.e., compare Fig. 1a with Fig. 1c).

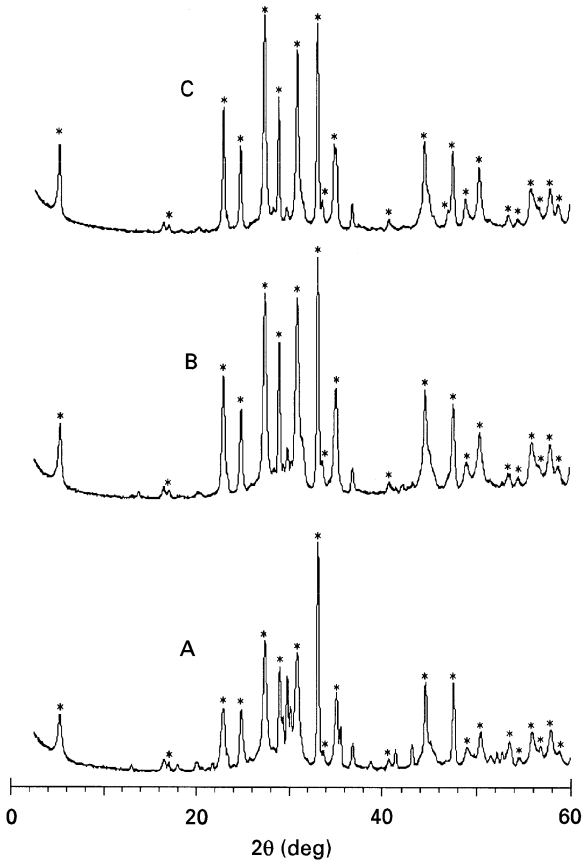

Figure 1 XRD patterns of BSCCO samples with the 2212 stoichiometry after calcination at 750 °C (curve A) followed by sintering at 820 °C for 12 h and at 855 °C for 1 h (curve B) and 100 h (curve C). The asterisks indicate peaks corresponding to the 2212 superconducting phase.

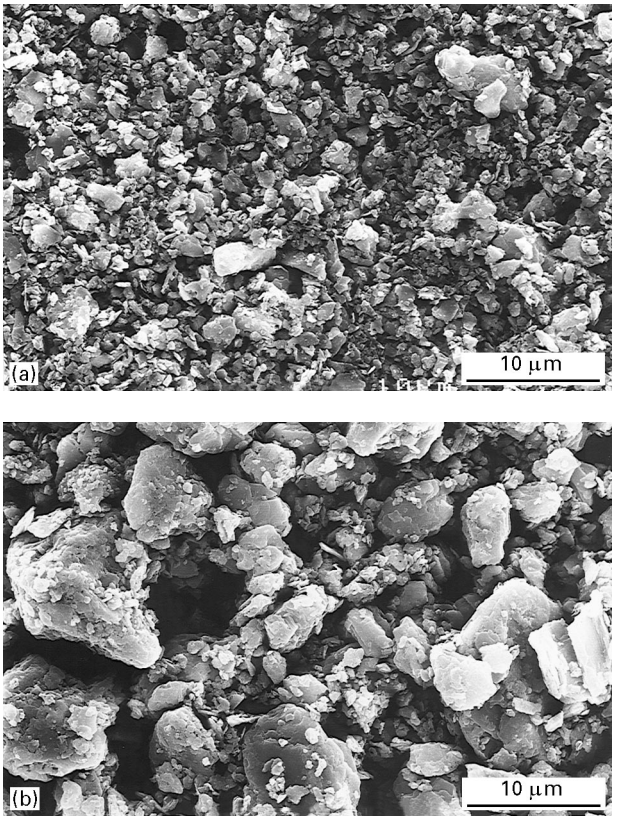

Figure 2 Secondary-electron scanning electrons micrographs obtained on BSCCO (2212) powdered samples after sintering at 855 °C for (a) 1 h (a) and (b) 3 h.

TABLE I Summary of the results obtained by XRD, SEM–EDS analysis and magnetic measurements on BSCCO (2 2 1 2) samples after calcination at 750 °C and milling followed by sintering at 820 °C for 12 h and at 855 °C for the different lengths of time indicated

Time (h)	Amount of 2212 (wt%)	T_{on} (K)	T_{cM} (K)
0	75	85	80.8
1	86	92	89.1
3	87	92	89.5
6	88	93	90.2
12	90	93	90.7
60	92	94	91.4
100	93	94	91.4

3.2. Scanning electron microscopy

The SEM images shown in Fig. 2a and b correspond to powdered samples sintered at 855 °C for 1 h and 3 h, respectively. Clear differences can be observed with respect to particle size and morphology between these samples. A significant particle size increase is observed during the initial 3 h of sintering, while only minor changes are observed thereafter. The morphology of the particles (Fig. 2b), which appear as elongated platelets (about 5–10 μm in size) with no preferential orientation, is representative of samples sintered for more than 3 h. Unequally large and small particles are observed in all the samples, indicating that growth of large grains takes place at the expense of smaller grains. In fact, as the sintering time is increased from 1 to 3 h, large grains are observed to increase significantly in size, while small grains decrease accordingly. These changes are not so clearly distinguished after sintering for more than 3 h, where much smaller changes in particle size are detected as a function of sintering time, consistent with the XRD results which suggest that mainly crystallinity changes occur at this stage.

A high degree of homogeneity in particle size has been observed throughout polished polycrystalline samples by SEM. This level of homogeneity is also maintained in the sample's chemical composition, as confirmed by EDS analysis, where the secondary phases identified also confirmed the results obtained by powder XRD. SrO_2, CuO, $SrCO_3$, Ca_2PbO_4, $CaCO_3$, Bi_2O_3, Bi_2CuO_4, $CaCu_2O_3$, Cu_2O and $3Bi_2O_3 \cdot 7CaO$ are found in the samples after calcination, in agreement with previously reported results [20–23]. A smaller amount of secondary phases is observed in sintered samples. These include $Sr_{14}Cu_{24}O_{41}$, Ca_2PbO_4, $CaCO_3$, Bi_2O_3, Bi_2CuO_4, $CaCu_2O_3$, Cu_2O and $3Bi_2O_3 \cdot 7CaO$. This non-superconducting phase decrease is accordingly accompanied by increased percentages of the 2212 phase content, as shown in Table I.

3.3. Magnetic characterization

The evolution of the superconducting properties along the synthesis process has been followed by means of $\chi_{a.c.}(T)$ measurements (Fig. 3). Even in the powders calcined at 750 °C (full circles), the diamagetism induced by the presence of a small amount of 2212 superconducting phase is already detected in the figure. After the first sintering step of 12 h at 820 °C, the major superconducting phase detected is 2212, although an increase in T_c is not yet observed (full squares). The second milling process combined with sintering at higher temperatures, initially 855 °C (1–3 h), results in a significant T_c increase accompanied by minor changes in the $\chi'(T)$ behaviour. Powders obtained after the first sintering at 820 °C have a density, ρ, about half the value of those samples sintered at 855 °C, while the ρ values remain essentially constant after the first hour. The simultaneous increase in T_{cM} and ρ with the sintering time would explain the crossing behaviour of the $\chi'(T)$ curves below T_{cM}, where steeper slopes of $\partial\chi'/\partial T$ are also associated with longer sintering processes.

There is a clear relationship between the sintering time at 855 °C and the evolution of $\chi_{a.c.}(T)$. The critical temperature increases above 80 K after the sample is calcined and sintered at 820 °C. Values of T_{on} above 93 K and of T_{cM} above 91 K are obtained after a subsequent sintering schedule of only 12 h. Further increases in sintering time do not yield substantial improvements in critical temperatures. In fact, within the experimental times of Table I, a logarithmic variation is observed, which seems to reach a saturation value of around 91.4 K for T_{cM} and 94 K for T_{on}. These values are among the highest found in the literature for the 2212 phase [12–14], with the added advantage that the synthesis method used is simple and the required processing time is not excessive.

$M(T, H)$ measurements have been performed at 5 and 20 K and representative results for 1 and 100 h are presented in Fig. 4. Main changes in the hysteresis loops are observed at the lowest temperatures and appear within 1–3 h of treatment, while only minor variations have been observed after sintering for 3 h. Differences still remain at 20 K, although to such a small extent that they cannot be observed at the scale represented in Fig. 4, where the ascending $M(H_+)$ and descending $M(H_-)$ loop branches merge at higher fields (the highest field used in the experiment is lower than the irreversibility field at this temperature). By comparing the limiting cases (1 and 100 h) it is clear that an increase in the sintering time leads to a small increase in the loop's width, $\Delta M(H) = M(H_+) - (M(H_-)$. This can be a consequence of larger grain size and of an increase in the amount of the superconducting phase, rather than an improvement in the intragranular critical currents.

These ideas have been tested analysing the field dependence of the critical current density, $J_c(H)$, which is proportional to $\Delta M(H)$. Moreover, to avoid the dependences on superconducting phase concentration, grain size distribution and density of the sample, the $J_c(H)$ values have been scaled with those obtained at zero field and the result presented in Fig. 5. Values in the low-field region have been discarded because the approximation $J_c(H) \propto \Delta M(H)$ holds only when the field has fully penetrated the sample. In all cases, the experimental points at 5 K may be fitted with the following relation:

$$\frac{J_c(H)}{J_c(H)} = \frac{1}{1 + (H/H_m)^{\beta}}$$

where H_m and β are fitting parameters. At 5 K, the samples sintered for 1 h at 855 °C yield values of $\beta = 0.87 \pm 0.01$ and $H_m = 7.2 \pm 0.1$ kOe. After 3 h 855 °C all samples exhibit a very similar behaviour, with weak improvement in $J_c(H)$ for fields higher than 10 kOe and values of $\beta = 0.69 \pm 0.01$ and

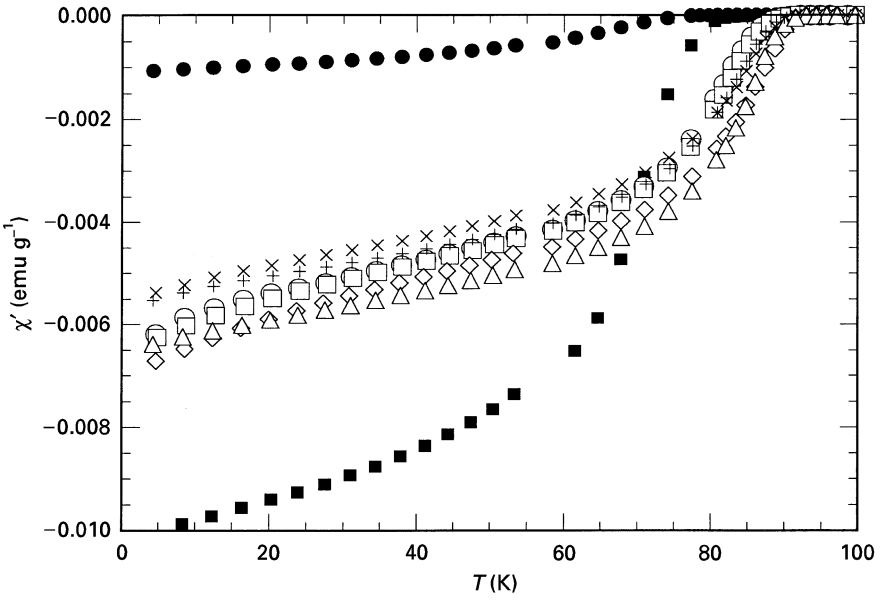

Figure 3 Temperature dependence of the in-phase component, $\chi'(T)$, of the magnetic a.c. susceptibility on powdered samples after calcination at 750 °C (●), first sintering at 820 °C for 12 h (■) and second sintering at 855 °C for 1 h (○), 3 h (□), 6 h (+), 12 h (×), 60 h (◇) and 100 h (△).

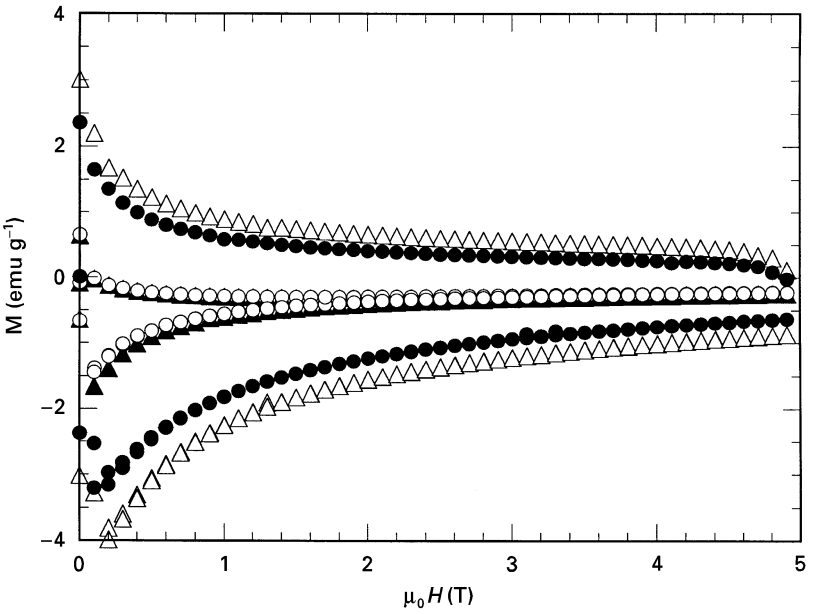

Figure 4 D.c. magnetization loops at 5 K (wider loops) and 20 K (narrower loops) for BSCCO (2212) samples sintered for 1 h (○, ●) and 100 h (△, ▲) at 855 °C.

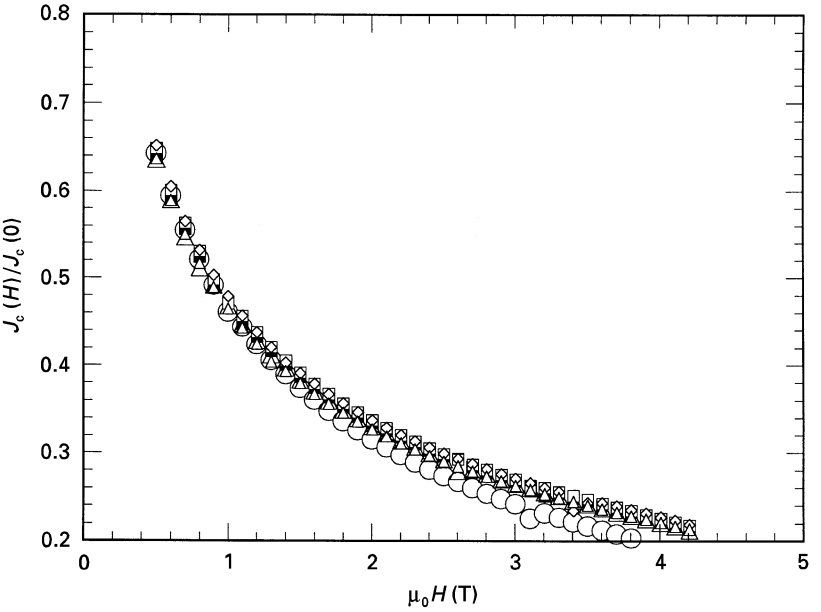

Figure 5 Scaled values for the critical current density $J_c(H)$ deduced from the magnetization loops at 5 K for the BSCCO (2212)-rich samples, after sintering a 855 °C for various times. (○), 1 h; (■), 3 h; (△), 6 h; (□), 12 h; (◇), 60 h; (△), 100 h.

$H_m = 5.1 \pm 0.1$ kOe. This dependence is close to the potential dependences that have been measured in this compound at low temperatures.

4. Applicability for textured materials

In order to develop technological applications, different textured materials have been fabricated using the above powders as precursors. The texture has been obtained inducing thermal gradients in the samples by means of two floating-zone methods: laser-floating zone (LFZ) [24, 25] and radio-frequency (r.f.) induction zone melting [26].

The LFZ system yields samples in which the superconducting grains grow with their *a–b* planes nearly parallel to the main axis of the sample. An example of the microstructure of LFZ-textured samples can be observed in Fig. 6a where micrographs of a sample before annealing are presented. Because of the high thermal gradients imposed by the use of a narrowly focused laser beam, this system allows the use of high growth speeds. For instance, recently grown samples 100 mm long and of 1 mm diameter reach transport critical current densities of 3500 A cm^{-2} at 77 K and zero external field.

These powders have also been used to fabricate Ag-sheathed BSCCO wires by the powder-in-tube method. As has been shown earlier, longer sintering times lead to slightly higher critical temperatures, but the intragranular properties are similar even after of sintering for only 1 h. In this context, powders sintered for 1 and 12 h were thus used to investigate whether the differences in starting powders influence the final properties of the wires. This may be important in

consideration of the practical potential of these wires for technological applications.

Wire fabrication details have been previously published [26]. In the mechanical plastic deformation process, the initial steps of the wire diameter reduction have been performed with a rotary swaging machine.

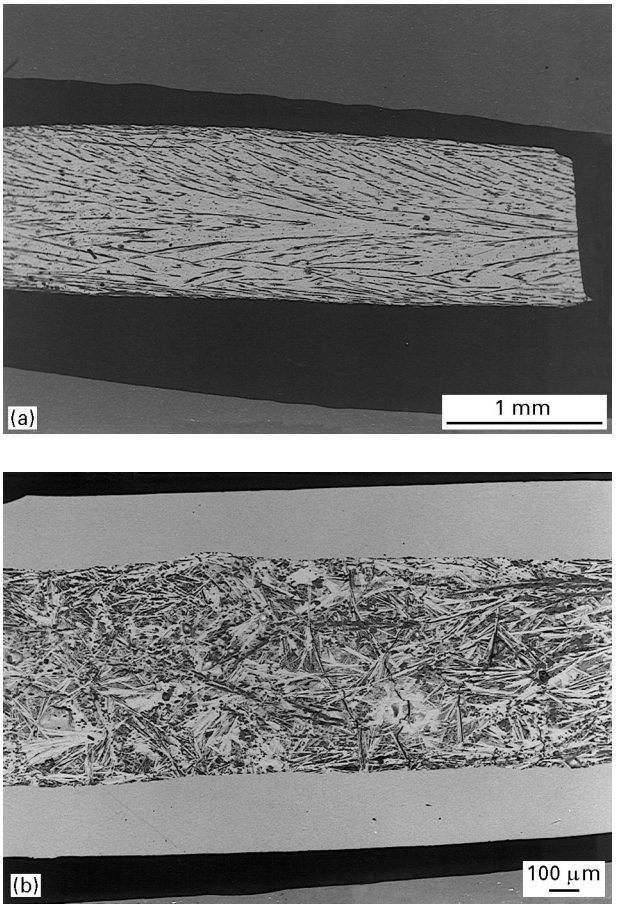

Figure 6 Typical microstructure of the samples grown with (a) the LFZ and (b) the r.f. inductor apparatuses before annealing. The sample in (a) has been grown using a rate of 30 mm h^{-1} while for the sample in (b) 15 mm h^{-1} was used.

Swaging reduces the size of the powder to below 1 μm in both cases. Texture is induced by means of a moving local r.f. induction zone melting apparatus and an example of the microstructure is presented in Fig. 6b. As this process entails melting of the ceramic inside the metal tube, it can be expected that the final properties of the wire should be independent of the initial powder, probed that there are no stoichiometry changes. This can be observed in Fig. 7, where the high-temperature region of the $\chi_{a.c.}(T)$ curve is presented for the wires and corresponding powders. An a.c. field amplitude of 5.5 Oe and a frequency of 119 Hz were used for powder measurements. In the case of the wires, the frequency was decreased to 11.9 Hz in order to reduce the contributions associated to eddy currents induced in the Ag sheath. The wires have a length of 1 cm and their diameters were measured using transverse scanning electron micrographs. In order to obtain non-dimensional susceptibilities and have the possibility of comparison between different wires, the signal in electromagnetic units has been divided by the superconducting volume. From the results presented in Fig. 7, it can be noticed that, even when the starting powder behaviours are different, both wires have an identical behaviour, very similar to that observed for the powder sintered for 12 h. It must be kept in mind that, after zone melting, the wire has been annealed for 12 h.

An important conclusion that can be deduced from the results presented here is that, since this wire fabrication method includes a melting process, starting powders obtained after only a short sintering time can be used to obtain wires with optimum properties. Wire annealing is of much greater importance, in this case, than the effects observed owing to the differences in characteristics of the starting powders produced by the polymer matrix procedure, whether they have been sintered for 1 or 100 h.

Furthermore, from results presented here and others described elsewhere, this superconductor is

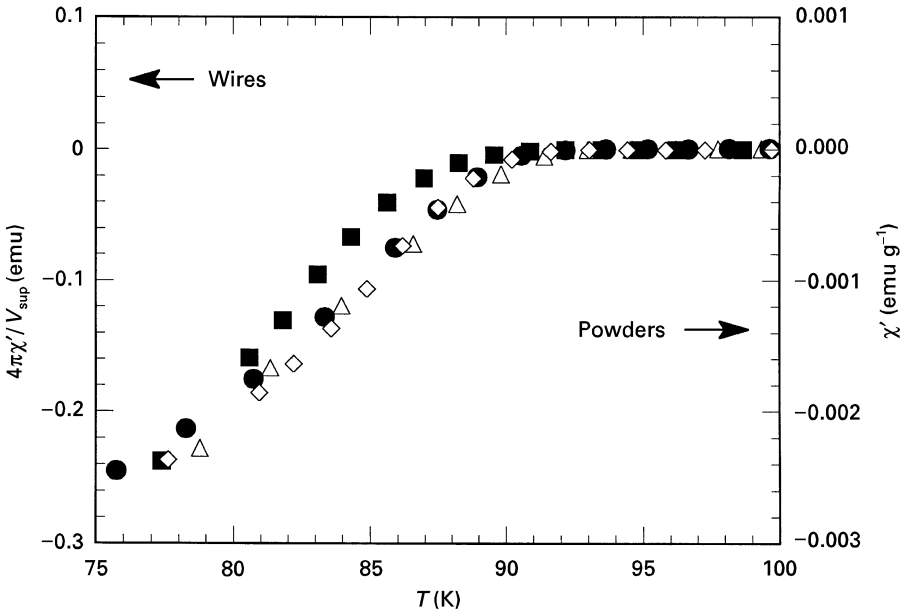

Figure 7 $\chi_{a.c.}(T)$ measurements performed on starting powders sintered for 1 h (■) and 12 h (◇), as well as the corresponding wires ((●), 1 h; (△), 12 h) obtained from these powders after the fabrication procedure outlined in the text.

considered to offer several advantages over the 2223 phase. Among them are its improved stability to moisture, faster preparation and higher degrees of phase purity and homogeneity. On the other hand, its lower critical temperature poses an important disadvantage when considering its potential for devices operating at 77 K. Nevertheless, since a number of important near-term applications for these high-T_c materials are being considered at temperatures below 65 K, the study of the 2212 phase superconductor and its reliable preparation are both of significant importance at this time.

5. Concluding remarks

A convenient synthetic method that yields a lead-free 2212 superconductor in air in a relatively short sintering time has been presented. The evolution of different microscopic and macroscopic characteristics have been followed as a function of the sintering time. The presence of the 2212 phase as the majority phase has been observed just after calcination, milling and initial sintering at 820 °C. After a second sintering treatment at 855 °C for 12 h, it reaches a concentration of 90 wt%. From the analysis of the magnetic behaviour it can be deduced that in the first few hours of sintering at 855 °C there is a parallel increase in the grain size, amount of 2221 phase and enhancement of the $J_c(H)$ behaviour, reaching T_{on} values above 93 K after treatment for 12 h. Moreover, times longer than 12 h result in only minor improvements.

Finally, the saturation of the total amount of 2212 phase content for sufficiently short sintering times, which is also clearly reflected in the superconducting characteristics, T_{on}, T_{cM} and $J_c(H)$, indicates a high stability for the 2212 phase grains grown. This synthetic method may thus be advantageous for the preparation of powders useful for further processing into shaped components (wires and tapes) displaying high critical current densities, which are currently under study.

Acknowledgements

This research has been supported by Programme MIDAS (Comisión Interministerial de Ciencia y Tecnologia oficina de coordinación y Desarrollo Electrotécnico-Red Eléctrica de España S.A.-unidad Eléctrica S.A.) projects 93/2231 and 94/2442 and by Comisión Interministerial de Ciencia y Tecnología projects MAT92-0896-C02-01 and 02. The authors acknowledge the technical assistance of J. Blasco from the Extended X-ray Absorption Fine-Structure Service, C. Gallego from the Electron Microscopy Service and the help of E. Martínez with the SQUID magnetometer, all of them available at the University of Zaragoza. General technical assistance with the floating-zone apparatuses is acknowledged from C. Estepa (Instituto de Ciencia de Materiales de Aragón).

References

1. C. MICHEL, M. HERVIEU, M. BOREL, A. GRANDIN, F. DESLANDES, J. PROVOST and B. RAVEAU, *Z. Phys. B.* **68** (1987) 421.
2. H. MAEDA, Y. TANAKA, M. FUKUTOMI and T. ASANO, *Jpn J. Appl. Phys.* **27** (1988) L209.
3. P. MAJEWSKI, *Adv. Mater.* **6** (1994) 460.
4. P. MAJEWSKI, H. L. SU and B. HETTICH, *Adv. Mater.* **4** (1992) 508.
5. D. BELTRÁN, M. T. CALDÉS, R. IBÁÑEZ, E. MARTÍNEZ, E. ESCRIBÁ, A. BELTRÁN, A. SEGURA, V. MUÑOZ and J. MARTÍNEZ, *J. Less-Common Metals* **150** (1989) 247.
6. D. C. SINCLAIR, J. T. S. IRVINE and A. R. WEST, *J. Mater. Chem.* **2** (1992) 579.
7. S. KAMBE, T. MATSUOKA, T. TAKAHASHI and M. KAWAI, *Phys. Rev. B* **42** (1990) 2669.
8. N. H. WANG, C. M. WANG, H. C. KAI, D. C. LING, H. C. KU and K. H. LU, *Jpn J. Appl. Phys.* **28** (1989) L1505.
9. S. K. AGARWAL, V. P. S. AWANA, V. N. MOORTHY, P. MARUTHI KUMAR, B. V. KUMARASWAMY, C. V. NARASIMHA RAO and A. V. NARLIKAR, *Physica C* **160** (1989) 278.
10. S. C. BHARGAVA, A. SEQUEIRA, J. S. CHAKRABARTY, H. RAJAGOPAL, S. K. SINHA and S. K. MALIK, *Solid State Commun.* **83** (1992) 905.
11. V. P. S. AWANA, S. B. SAMANTA, P. K. DUTTA, E. GMELIN and A. V. NARLIKAR, *J. Phys.: Condens. Matter* **3** (1991) 8893.
12. A. C. VAJPEI and G. S. UPADHYAYA (eds) *Key Engng Mater.* **75–76** (1992).
13. G. TRISCONE, J. Y. GENOUD, T. GRAF, A. JUNOD and J. MULLER, *Physica C* **176** (1991) 247.
14. J. M. GONZÁLEZ-CALBET, A. BADÍA, M. VALLET-REGÍ, A. CANEIRO, J. RAMIREZ, C. RILLO, F. LERA and R. NAVARRO, *Physica C* **203** (1992) 223.
15. A. SOTELO, G. F. DE LA FUENTE, F. LERA, D. BELTRÁN, F. SAPIÑA, R. IBÁÑEZ, A. BELTRÁN and M. R. BERMEJO, *Chem. Mater.* **5** (1993) 851.
16. A. SOTELO, PhD thesis, Universidad de Zaragoza (1994).
17. M. T. RUIZ, G. F. DE LA FUENTE, A. BADÍA, J. BLASCO, M. CASTRO, A. SOTELO, A. LARREA, F. LERA, C. RILLO and R. NAVARRO, *J. Mater. Res.* **8** (1993) 1268.
18. A. SOTELO, L. A. ANGUREL, M. T. RUIZ, A. LARREA, F. LERA and G. F. DE LA FUENTE, *Solid State Ionics* **63–65** (1993) 889.
19. C. RILLO, F. LERA, A. BADÍA, L. A. ANGUREL, J. BARTOLOMÉ, F. PALACIO, R. NAVARRO and A. J. VAN DUYNEVELDT, in "Magnetic susceptibility of superconductors and other spin systems", edited by R. A. Hein, T. L. Francavilla and D. H. Liebenberg (Plenum, New York, 1991) pp. 1–24.
20. R. S. ROTH, C. J. RAWN, J. J. RITTER and B. P. BURTON, *J. Amer. Ceram. Soc.* **72** (1989) 1545.
21. B. P. BURTON, C. J. RAWN and R. S. ROTH, *J. Res. Natl Inst. Stand. Technol.* **98** (1993) 469.
22. K. SCHULZE, P. MAJEWSKI, B. HETTICH and G. PETZOW, *Z. Metallkde* **81** (1990) 836.
23. J. SESTÁK, *J. Therm. Anal.* **36** (1990) 1639.
24. L. A. ANGUREL, G. F. DE LA FUENTE, A. BADÍA, A. LARREA, J. C. DÍEZ, J. I. PEÑA, E. MARTÍNEZ and R. NAVARRO, in "Studies of high temperature superconductors", Vol. 20, edited by A. Narlikar (Nova Science, Publishers, New York, 1997) pp. 1–31.
25. G. F. DE LA FUENTE, J. C. DÍEZ, L. A. ANGUREL, J. I. PEÑA, A. SOTELO and R. NAVARRO, *Adv. Mater.* **7** (1995) 853.
26 J. I. PEÑA, L. A. ANGUREL, A. SOTELO, G. F. DE LA FUENTE and R. NAVARRO, in Proceedings of the Fourth Conference of the European Ceramic Society, Vol. 8 Superconductivity and Superconducting Materials Technologies, October 1995, edited by P. Vicenzini (Techna, Faenza, 1995) pp. 481–488.

Received 4 October 1996
and accepted 1 May 1997